

Collapse of turbulence in curved pipe flow

Eman Bagheri,* Stefan Becker, and Philipp Schlatter
*Institute of Fluid Mechanics (LSTM),
 Friedrich-Alexander-Universität (FAU) Erlangen-Nürnberg,
 DE-91058 Erlangen, Germany*

Turbulence-induced friction is a significant contributor to energy consumption in the fluid-transport and piping industries. Here, we describe a passive approach to suppress turbulence and reduce friction: we show that a local increase in streamwise flow curvature, combined with changing the circular cross-section to an oval, relaminarizes turbulent flow in curved pipes. We exemplify this effect in a 180° bend at $Re_D = 10000$ and 20000 , well above the linear stability limit. Curvature inhibits streamwise Reynolds stresses, and cross-sectional modifications weaken the unstable secondary flow, together disrupting the near-wall regeneration cycle and collapsing turbulence. Simulations and experiments confirm that these geometric modifications suppress turbulence and reduce pressure loss by 53% and 36% compared to the baseline 180° bend and a fully developed straight pipe of equal length, respectively. The results establish a passive, mechanism-based route to relaminarization in curved pipes with implications for energy-efficient control in other wall-bounded flows with curvature.

In most applications, a key objective is to reduce turbulence as much as possible because of its adverse effect on frictional losses. It has been demonstrated previously that by appropriately modifying the mean profile of a turbulent pipe flow, partial or full relaminarization may be achieved [1–3]. In curved pipes, frictional losses are even more pronounced, given the thinner shear layers on the outer side of the bend, coupled with geometry-induced in-plane motion. Flow in curved pipes is integral to applications such as heat exchangers, biological systems (e.g. the aortic arch), and fluid transport networks, where turbulence-induced frictional loss remains a major contributor to global energy consumption [4–6]. Despite more than a century of research, several open questions related to curved-pipe flows remain. From the seminal contributions of Dean [7, 8], it is well established that curvature induces a secondary flow, the so-called Dean vortices. Subsequently, White [9] and Taylor [10] studied turbulence and transition in curved pipes and discovered that curvature fundamentally changes both the onset and the dynamics of turbulence. Although the influence of curvature on transition and turbulence has been studied and partial curvature-induced flow relaminarization has since been reported several times in the literature [11, 12], the underlying mechanisms that can suppress turbulence are not yet well understood. In this context, two important open questions remain: Can geometric features disrupt the turbulence regeneration cycle and restore laminar flow beyond the stability limit? If so, through what physical mechanisms is relaminarization achieved?

As energy consumption and pumping power have long been of major concern, the focus of many earlier studies was the quantification of the friction factor and pressure loss. Ito [13] made fundamental contributions by providing widely used empirical correlations for the friction factor and the bend loss coefficient in smooth bent pipes as functions of Reynolds number and curvature. Sreenivasan and Strykowski [11] then provided experimental ev-

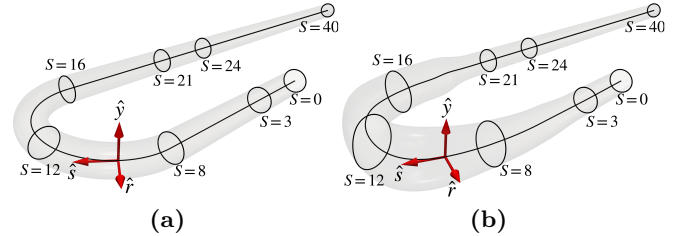


Figure 1. (a) Baseline bend (BL, $\gamma = 0.2$) (b) optimized bend (OPT, variable γ with $\gamma_{\max} \approx 0.8$). Frenet–Serret frame with \hat{s} : tangent (streamwise); \hat{r} : radial (centrifugal); \hat{y} : binormal (lateral) unit vectors.

idence that curvature can stabilize turbulence in helically coiled pipes and even induce relaminarization at moderate Reynolds numbers. More recently, Kühnen et al. [14] confirmed Sreenivasan’s conclusion that a fully turbulent flow may be relaminarized due to curvature effects. Cioncolini and Santini [15] studied a wide range of non-dimensional curvatures ($\gamma = D/(2R_c) \simeq 0.0027 - 0.145$) and Reynolds numbers ($Re_D = U_B D/\nu \approx 10^3 - 6.3 \times 10^4$) and found that, outside of the transitional region, their data were generally in agreement with Ito’s correlations. Here, R_c denotes the centerline’s radius of curvature, D is the pipe diameter, and U_B represents the bulk velocity. However, for coils with curvature of $\gamma \simeq 0.01 - 0.03$, they reported a “depression” region in the friction–factor profile within which the curved–pipe friction factor is not necessarily higher than that of a straight pipe at the same Reynolds number (i.e. “substraight” behavior). Using direct numerical simulations (DNSs) at $\gamma = 0.01$, Noorani et al. [12] also found a substraight regime at $Re_D = 5300$. Noorani and Schlatter [16] subsequently discovered a regime “sublaminar” near $Re_D \approx 3400$ in long, mildly curved pipes ($\gamma = 0.01$), in which the mean drag was up to 8% below the laminar correlation. Furthermore, they observed that strong curvature ($\gamma = 0.1$) partially relaminarizes the flow near the inner wall. Consistently, earlier DNS of helically coiled pipes by Hüttl and Friedrich [17] also showed that strong curvature ($\gamma = 0.1$) suppresses tur-

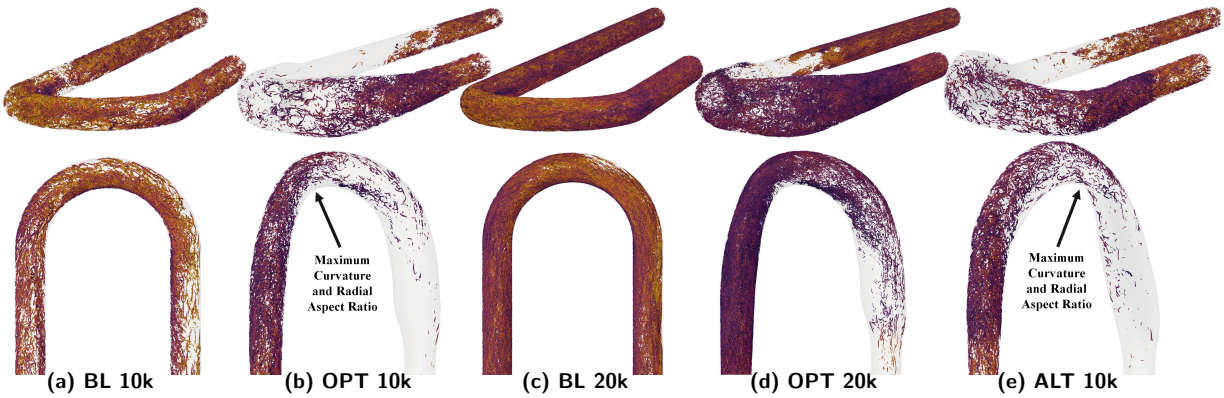


Figure 2. Isosurfaces of $\lambda_2 = -10 U_B^2 / D^2$, colored by velocity magnitude. (a,c) show the baseline design at $Re_D = 10000$ and $Re_D = 20000$, respectively. (b,d) In the optimized case at both Reynolds numbers, turbulence decays shortly after the bend entry at $s \approx 10$ up to the location where the cross section is constrained back to a circular shape at $s \approx 21$. (e) illustrates an alternative optimized shape corresponding to another local minimum, also leading to relaminarization.

bulence and can nearly relaminarize the flow. However, they also noted that the secondary flow can generate remarkably high local Reynolds shear stresses near the upper and lower walls, underscoring the impact of the secondary flow in sustaining turbulence. In transitional bent pipe flows, Rinaldi et al. [18] showed that curvature eliminates the strong upstream front of puffs and slugs and pushes the production region toward the outer wall. Overall, the curvature-induced relaminarizations in the literature are reported at low Reynolds numbers ($Re_D \approx 3 \times 10^3 - 6 \times 10^3$). Canton et al. [19] indicate that these low Reynolds number stabilizing effects observed in moderate-curvature regimes are attributed to the linear stability threshold in curved pipes, rather than a turbulence suppression mechanism. At higher Re_D , only the inner wall region partially relaminarizes while the overall friction factor remains higher than that of the straight pipe.

Previous studies have established that turbulence in curved pipes is governed by Reynolds number and curvature. The collective evidence shows that curvature introduces competing mechanisms that can promote or suppress turbulence. Furthermore, it suggests that turbulence in curved pipes could potentially be controlled by geometric modifications. In this context, two aspects remain unexplored in the literature. Firstly, the evidence for relaminarization in curved pipes at high Reynolds numbers well beyond the linear stability limit is absent to the best of our knowledge. Secondly, the effect of the cross-sectional profile on the Dean vortices and their influence on turbulence is overlooked. The latter is crucial since a strong streamwise curvature can indirectly intensify turbulence by transferring energy from the primary flow to unstable Dean vortices. On the other hand, an appropriate cross-sectional shape modification can weaken the Dean vortices, thereby limiting their role in both the production and redistribution of turbulence.

We address these two aspects by investigating whether relaminarization of turbulent flow can be achieved through

geometric modification of the pipe, thereby unlocking the potential for lower drag forces in general piping systems. We consider the combined modification of the local centerline curvature and the cross-sectional geometry. Rather than performing a parametric study of local curvature and cross-sectional profile within a high-dimensional geometric space, we pose and solve an automatic optimization problem using the method described in [20, 21] to determine the required changes in these two geometric variables. We then analyze the resulting optimal flow to identify the underlying physical mechanisms that relaminarize the flow. The objective function to be minimized is the total entropy generation in the flow, as a measure of the appearance of turbulence. For incompressible and isothermal flows, entropy generation is due to viscous dissipation, and our objective function can be defined as

$$J = \int_{\Omega} \Phi dV = \int_{\Omega} (\tau : \nabla U + \rho \varepsilon) dV, \quad (1)$$

where τ is the mean viscous stress tensor, ∇U the mean velocity gradient, and ε denotes the modeled turbulent dissipation. We minimize irreversible losses in the flow [22, 23], thus biasing the search toward low-dissipation laminar states. Using DNS, we then verify whether these geometric modifications can achieve relaminarization. The optimization is carried out for a baseline 180° bend (BL) at $Re_D = 10000$ with $\gamma = 0.2$, as illustrated in Fig. 1(a). The resulting optimal design (OPT), after 50 automatic design iterations, is shown in Fig. 1(b). Only the segment located between arc length $s = 3$ and $s = 21$ is subject to optimization, and the rest of the geometry ($s < 3$ or $s > 21$) is constrained to remain unchanged. The DNS was performed at $Re_D = 10000$ and 20000 for both geometries using the highly accurate spectral element method with a polynomial degree of seven. All simulations employ fully-developed turbulent inflow conditions as described in [24]. Furthermore, the DNS results were experimentally validated against pressure loss measurements obtained from a pair of differential pressure sensors located at $s = 0$ and $s = 24$. The DNS results confirm that the modi-

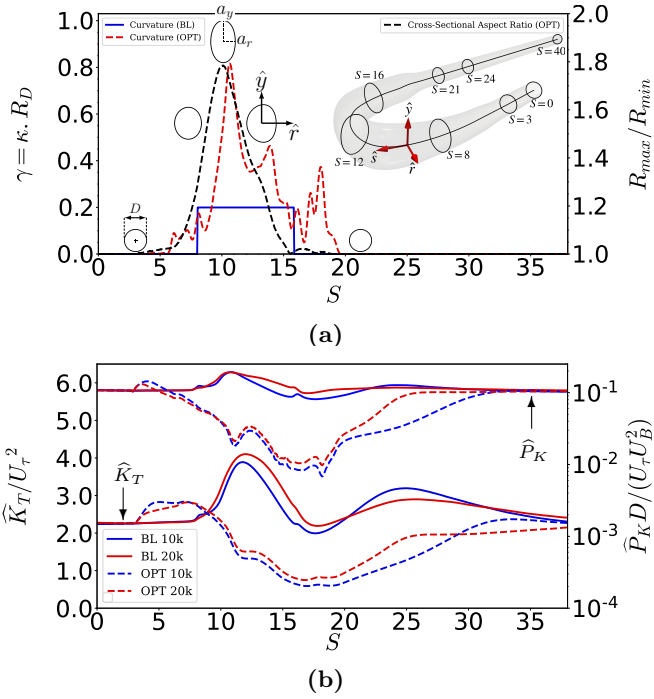


Figure 3. (a) Geometric characteristics of baseline and optimized bends: left axis shows non-dimensional curvature and right axis the cross-sectional aspect ratio (i.e. ratio of principal axes). Representative cross-sectional shapes are shown for clarity. (b) Cross-sectionally averaged TKE (\hat{K}_T) on the left axis, with its production (\hat{P}_K) shown on the right axis in logarithmic scale. U_τ denotes the wall friction velocity.

fied geometry attains near full relaminarization at both Reynolds numbers. Fig. 2(b) and (d) illustrate visually that turbulent structures convected from the inflow region begin to decay near $s \approx 10$ in the modified design (see the baseline design in Fig. 2(a) and (c) for comparison). Note that both Reynolds numbers are well above the linear stability limit [25]. Moreover, the optimization results in multiple families of solutions, each converging to a distinct local minimum. For instance, Fig. 2(e) shows an alternative modified geometry at $Re_D = 10000$ (ALT 10k). This shows that the geometric modification required to achieve relaminarization is not unique. Despite clear differences, both modified geometries have a key feature in common that relaminarizes the flow. In both cases, the maximum local curvature coincides with a large cross-sectional aspect ratio where turbulence starts to decay. For brevity, we do not further discuss geometry ALT in this letter.

Fig. 3(a) shows the centerline curvature and the cross-sectional aspect ratio of the modified and baseline geometries and underlines two major characteristics of the modified geometry. Firstly, the centerline curvature significantly increases from 0.2 in BL to 0.82 in OPT at $s \approx 10$, consistent with previous findings [12, 17, 18] on the stabilizing effect of strong streamwise curvature. Secondly, the cross-sectional profile has an oval shape elongated in the binormal direction \hat{y} with the ratio of its principal axes

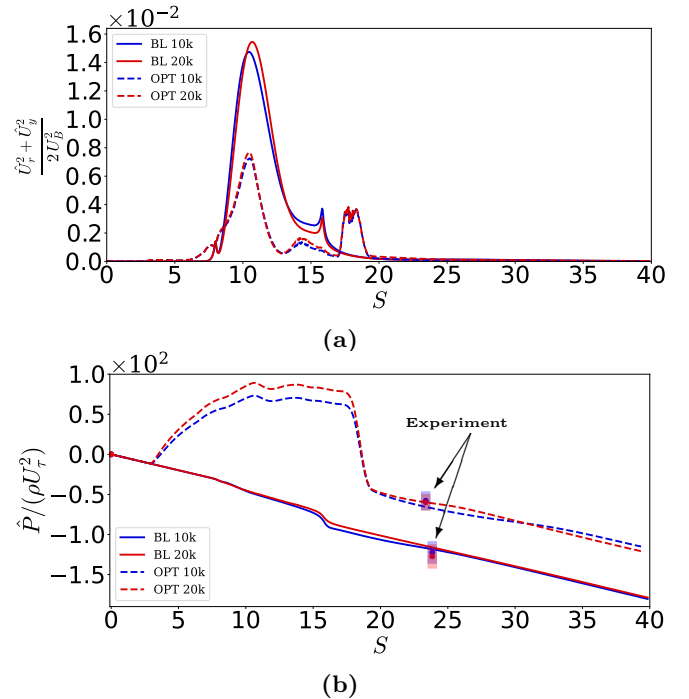


Figure 4. (a) Kinetic energy of the secondary flow. Despite a stronger curvature, the modified shape has a weaker secondary flow owing to its cross-sectional shape. (b) Streamwise mean pressure for BL and OPT at $Re_D = 10000$ and 20000. Markers indicate pressure loss measurements, and shaded bands denote one standard deviation ($\pm\sigma$), accounting for turbulent fluctuations and measurement uncertainty.

reaching a maximum of $R_{\max}/R_{\min} = 1.78$ near $s \approx 10$. Note that both the curvature and the cross-sectional aspect ratio reach their maximum nearly simultaneously at $s \approx 10$. We analyze the impact of these two geometric modifications by deriving the Reynolds-averaged equations in the Frenet-Serret coordinate system shown in Fig. 1 (see the supplemental material for the derivation and equations). We adopt this frame with unit vectors \hat{s} (tangent/streamwise), \hat{r} (radial/centrifugal), and \hat{y} (binormal/lateral), rather than the common toroidal coordinate system as the mean flow lacks azimuthal homogeneity, and flow dynamics in the radial and binormal directions differ fundamentally. The arc length s is non-dimensionalized by the straight pipe diameter D . In this frame, we define the cross-sectional average of a time-averaged field $g(r, y, s)$ as

$$\hat{g}(s) = \left[\iint_{\mathcal{A}(s)} g(r, y, s) dr dy \right] / \left[\iint_{\mathcal{A}(s)} dr dy \right], \quad (2)$$

where $\mathcal{A}(s)$ denotes the pipe's cross section in (r, y) plane at arc length s . Expressing all terms in this frame enables us to isolate and study the geometric effects. In Eq. (S1), $\kappa = 1/R_c$ denotes the centerline curvature and explicitly appears in the production of the streamwise Reynolds-stress equation. As fluid particles accelerate toward the outer wall under the centrifugal force, the radial velocity satisfies $U_r \geq 0$ everywhere except near the top and

bottom walls. Consequently, the first curvature term in

$$-2 \frac{\kappa}{h_s} (R_{ss} U_r + R_{sr} U_s) \quad (3)$$

has a stabilizing effect on the streamwise Reynolds stress R_{ss} by reducing its production everywhere, except in the thin regions in the vicinity of the upper and lower walls. The strength of this term is determined by the local curvature κ/h_s (with $h_s = 1 + \kappa r$), being strongest near the inner wall and weakest near the outer wall. The second term in Eq. (3) also appears in the production of radial stresses, with opposite sign and twice the magnitude (see Eq. (S2)). It locally exchanges energy between the streamwise and radial Reynolds stresses through the radial-streamwise shear stress and makes a net contribution to the production of turbulent kinetic energy (TKE). On the inner wall, it enhances the streamwise stress while reducing the radial stress, and its net effect suppresses the TKE production (see Eq. (S3)). This term has the opposite effect on the outer wall and is responsible for the localization of the TKE production toward the outer wall (see Rinaldi *et al.* [18]) and the inner wall partial relaminarization observed in [12]. At the same time, the curvature induces the unstable Dean vortices, contributing to the production of cross-stream Reynolds stresses. Moreover, the secondary flow redistributes the TKE produced on the outer wall by transporting turbulent structures into the core and toward the inner wall. Therefore, the streamwise flow curvature has both suppressing and enhancing effects on turbulence, and the balance between these competing mechanisms determines the net outcome.

Fig. 3(b) shows that TKE production initially increases at $s = 4$, intensifying the TKE from $s = 4$ to $s = 8$ in the optimized design. This is in line with the observation by Kühnen *et al.* [2] that the return to laminar motion is accomplished by initially increasing turbulence intensities. Following that, the production decreases exponentially from $s = 5$ to $s = 18$ at $Re_D = 10000$ (OPT 10k) and $Re_D = 20000$ (OPT 20k). As a consequence, the TKE steadily decays from $s = 8$ to $s = 18$. In contrast, the TKE production inside the baseline bend increases, resulting in 1.7 to 1.8 times higher peak TKE compared to the straight section. This is mainly due to the instability of the secondary flow, which generates cross-stream Reynolds stresses (R_{yy} and R_{rr}) and raises the overall turbulence intensity. In straight pipes, these two components arise primarily through redistribution by the pressure-strain, whereas in curved pipes, they are directly amplified by the production terms P_{yy} and P_{rr} (see Eq. (S4) and Eq. (S2)). The increase in cross-stream Reynolds stresses intensifies the shear-stress production P_{sy} and P_{sr} through $R_{yy} \partial_y U_s$ and $R_{rr} \partial_r U_s$ (see Eq. (5) and (6)). The intensified shear stresses feed back into the production of streamwise stress R_{ss} through $R_{sy} \partial_y U_s$ and $R_{sr} \partial_r U_s$ (see Eq. (7)), counteracting the stabilizing curvature effects, thereby regenerating streaks and sustaining turbulence.

This mechanism explains why previous studies have not reported relaminarization at higher Reynolds numbers merely through curvature modifications without changing the cross-section. Our complementary wall-resolved LES of circular bends, matched to the optimal local curvature and local Dean number, confirms the absence of relaminarization when the cross section remains circular. As shown in the mean streamwise vorticity Eq. (S5), the binormal gradient of the centrifugal force

$$\partial_y \left(\frac{\kappa}{h_s} U_s^2 \right) \sim \frac{1}{a_y} \frac{\kappa \hat{U}_s^2}{h_s} \quad (4)$$

is the main driving term of the Dean vortices. Hence, increasing the curvature without modifying the cross-sectional profile results in stronger Dean vortices. The instability of the Dean vortices, in turn, sustains the turbulence inside the bend through cross-stream Reynolds stresses. Near the inner wall, the major principal axes of both the Reynolds stress and production tensors become closely aligned with the binormal direction, and R_{yy} emerges as the primary carrier of turbulence.

The optimized design counters this effect by ovalizing the cross section and increasing the lateral half-width a_y as curvature increases (see Fig. 3(a)). Enlarging the cross-sectional area reduces the averaged streamwise velocity \hat{U}_s , and together with the increase in the lateral half-width a_y weakens the driving term of the unstable Dean vortices in Eq. (4). As a direct consequence, Fig. 4(a) shows a 50% reduction in the peak kinetic energy of the secondary flow relative to the baseline geometry. By reducing the energy of the Dean vortices, cross-stream Reynolds stress components R_{yy} and R_{rr} diminish. The leading terms in shear-stress productions are

$$P_{sy} \approx -R_{yy} \partial_y U_s - R_{yr} \partial_r U_s, \quad (5)$$

$$P_{sr} \approx -R_{ry} \partial_y U_s - R_{rr} \partial_r U_s + \frac{\kappa U_s}{h_s} (2R_{ss} - R_{rr}). \quad (6)$$

With scaling $\partial_y U_s \sim \hat{U}_s/a_y$, the increase in a_y due to ovalization reduces the binormal mean velocity gradient in the production of shear stresses without affecting the curvature factor κ/h_s . Reducing cross-stream stresses (R_{yy} and R_{rr}) and the binormal mean velocity gradient $\partial_y U_s$ suppress the shear-stress productions in Eq. (5) and (6). As shear stresses R_{sr} and R_{sy} are subdued, the streamwise production P_{ss} in Eq. (7) drops, and the near-wall streaks diminish.

$$P_{ss} = -2 \left[R_{ss} \frac{\partial_s U_s + \kappa U_r}{h_s} + R_{sy} \partial_y U_s + R_{sr} \left(\partial_r U_s + \frac{\kappa U_s}{h_s} \right) \right] \quad (7)$$

The combined effect of increased streamwise curvature and the weaker secondary motion suppresses turbulence and reduces the mean velocity gradient. Consequently, the optimized bend achieves a 53% reduction in pressure

loss relative to the baseline bend, confirmed by experiment (Fig. 4(b)). Due to relaminarization, its pressure loss is 36% below that of a fully developed straight turbulent pipe of equal length at the same Reynolds number. Furthermore, based on our pressure loss measurements, this behavior persists at higher Reynolds numbers beyond $Re_D = 20000$. As shown in Fig. 3(b), the primary difference in the TKE and TKE production of OPT 10k and OPT 20k is in the re-transition region beyond $s \approx 20$, where the geometry returns to a straight circular pipe due to the optimization constraint. At $Re_D = 20000$, the residual turbulent slugs near $s \approx 20$ grow more rapidly, and turbulence recovers faster in the straight section of the pipe (see Fig. 2(d) and Fig. 3(b)). Nevertheless, in the relaminarizing region from $s = 8$ to $s = 18$, the TKE and TKE production remain largely unchanged between OPT 10k and OPT 20k, indicating only a weak Reynolds-number dependence (see Fig. 3(b)).

The present work shares with Kühnen et al. [2] the main idea that turbulence can be suppressed by interrupting the self-sustaining near-wall cycle, but achieves it passively by geometric modifications. The cycle entails the following: streamwise rolls lift up the streaks, the streaks become unstable and break down, and the resulting fluctuations regenerate the rolls [26–28]. We disrupt this loop in the following way. Firstly, the strong streamwise curvature has a suppressing influence on the TKE production on the inner wall and reduces the production of streamwise Reynolds stress on the outer wall, hence the streaks are no longer reinforced. Secondly, an oval cross-section elongated in the binormal direction has two additional effects. By increasing the cross-sectional area and the lateral half-width, the centrifugal force and the centrifugal production of the secondary flow in the streamwise mean vorticity equation are reduced. This, in turn, weakens the unstable Dean vortices and decreases their energy feedback into turbulence via the cross-stream Reynolds stresses. In addition, through attenuation of the binormal mean shears and the cross-stream Reynolds stresses, it reduces the shear-stress productions and consequently weakens the shear stresses that reinforce the streaks. As both the direct energy and the feedback mechanisms are disrupted, streaks are suppressed, and turbulence collapses inside the bend.

The current work opens new avenues to control turbulence in pipe flow, and thus to reduce the friction imposed on the pipe walls. Given the novel insights into the budget equations of the turbulent kinetic energy, and its connection to both pipe curvature and cross section, new approaches in other situations are also possible.

Acknowledgment: This project was partially funded by the Bavarian research foundation under project No AZ-1232-16. The authors gratefully acknowledge the scientific support and HPC resources provided by the Erlangen National High Performance Computing Center (NHR@FAU) of the Friedrich-Alexander-Universität Erlangen-Nürnberg

(FAU). The hardware is funded by the German Research Foundation (DFG). This work has received funding from the European High Performance Computing Joint Undertaking (JU) and Sweden, Germany, Spain, Greece and Denmark under grant agreement No 101093393.

* eman.m.bagheri@fau.de

- [1] B. Hof, A. de Lozar, M. Avila, X. Tu, and T. M. Schneider, *Science* **327**, 1491 (2010).
- [2] J. Kühnen, B. Song, D. Scarselli, N. B. Budanur, M. Riedl, A. P. Willis, M. Avila, and B. Hof, *Nature Physics* **14**, 386 (2018).
- [3] D. Scarselli, J. Kühnen, and B. Hof, *Journal of Fluid Mechanics* **867**, 934 (2019).
- [4] S. A. Berger, L. Talbot, and L.-S. Yao, *Annual Review of Fluid Mechanics* **15**, 461 (1983).
- [5] S. Vashisth, V. Kumar, and K. D. P. Nigam, *Industrial & Engineering Chemistry Research* **47**, 3291 (2008).
- [6] A. Kalpakli Vester, R. Örlü, and P. H. Alfredsson, *Applied Mechanics Reviews* **68**, 050802 (2016).
- [7] W. R. Dean, *The London, Edinburgh, and Dublin Philosophical Magazine and Journal of Science* **4**, 208 (1927).
- [8] W. R. Dean, *The London, Edinburgh, and Dublin Philosophical Magazine and Journal of Science* **5**, 673 (1928).
- [9] C. M. White, *Proceedings of the Royal Society of London. Series A* **123**, 645 (1929).
- [10] G. I. Taylor, *Proceedings of the Royal Society of London. Series A* **124**, 243 (1929).
- [11] K. R. Sreenivasan and P. J. Strykowski, *Experiments in Fluids* **1**, 31 (1983).
- [12] A. Noorani, G. K. El Khoury, and P. Schlatter, *International Journal of Heat and Fluid Flow* **41**, 16 (2013).
- [13] H. Ito, *Journal of Basic Engineering* **81**, 123 (1959).
- [14] J. Kühnen, P. Braunshier, M. Schwegel, H. C. Kuhlmann, and B. Hof, *Journal of Fluid Mechanics* **770**, R3 (2015).
- [15] A. Cioncolini and L. Santini, *Experimental Thermal and Fluid Science* **30**, 367 (2006).
- [16] A. Noorani and P. Schlatter, *Physics of Fluids* **27**, 035105 (2015).
- [17] T. J. Hüttl and R. Friedrich, *International Journal of Heat and Fluid Flow* **21**, 345 (2000).
- [18] E. Rinaldi, J. Canton, and P. Schlatter, *Journal of Fluid Mechanics* **866**, 487 (2019).
- [19] J. Canton, P. Schlatter, and R. Örlü, *Journal of Fluid Mechanics* **792**, 894 (2016).
- [20] T. Albring, M. Sagebaum, and N. R. Gauger, in *AIAA Aviation Forum*, AIAA 2016-3518 (2016).
- [21] M. Sagebaum, T. Albring, and N. R. Gauger, *ACM Transactions on Mathematical Software* **45**, 1 (2019).
- [22] F. Kock and H. Herwig, *International Journal of Heat and Mass Transfer* **47**, 2205 (2004).
- [23] F. Kock and H. Herwig, *International Journal of Heat and Fluid Flow* **26**, 672 (2005).
- [24] L. Hufnagel, J. Canton, R. Örlü, O. Marin, E. Merzari, and P. Schlatter, *Journal of Fluid Mechanics* **835**, 86 (2018).
- [25] D. Massaro, V. Lupi, A. Peplinski, and P. Schlatter, *Physical Review Fluids* **8**, 113903 (2023).
- [26] J. M. Hamilton, J. Kim, and F. Waleffe, *Journal of Fluid Mechanics* **287**, 317 (1995).
- [27] J. Jiménez and A. Pinelli, *Journal of Fluid Mechanics* **389**, 335 (1999).
- [28] F. Waleffe, *Physics of Fluids* **9**, 883 (1997).